International Journal of Mechanical Sciences 88 (2014) 154–161

Contents lists available at ScienceDirect

International Journal of Mechanical Sciences

journal homepage: www.elsevier.com/locate/ijmecsci

Numerical investigation on mechanical properties of cellular lattice structures fabricated by fused deposition modeling

M.R. Karamooz Ravari *, M. Kadkhodaei, M. Badrossamay, R. Rezaei

Department of Mechanical Engineering, Isfahan University of Technology, 84156-83111 Isfahan, Iran

ARTICLE INFO

Article history:
Received 25 May 2014
Received in revised form
28 July 2014
Accepted 8 August 2014
Available online 17 August 2014

Keywords:
Cellular lattice structure
Fused deposition modeling
Beam finite element
Solid finite element
Elastic modulus
Collapse stress

ABSTRACT

Cellular lattice structures (CLS) with designed structural integrity are highly demanded in many applications such as light-weight industrial components and bone scaffold. In recent years, additive manufacturing (AM) processes have been found to be capable of producing such products with controllable porosity and pore sizes. However, AM faces an inherent obstacle so that the CLS strut diameter varies along its length. This study uses finite element modeling to predict the effect of variation in the struts' diameter on the elastic modulus as well as collapse stress of CLS using both beam and solid finite elements. To determine the mechanical behavior of the lattice and bulk material, lattice structures as well as compression test specimens are fabricated using fused deposition modeling. The results show that the beam finite element model is stiffer than the solid one since the beam model cannot capture the effects of material concentration at the points of diameter variations. However, the obtained elastic modulus does not differ significantly between solid and beam models while the difference is not negligible for collapse stress.

1. Introduction

Nowadays, lightweight and energy absorbent materials are of interest in several industries such as automobile, aerospace, and marine due to their notable mechanical properties. Among the lightweight materials, the cellular lattice structures are of more importance since the microstructure of the lattice is regular so that the achieved mechanical properties can be adjusted by using an appropriate structure. In recent years, additive manufacturing (AM) methods have been widely used by researchers worldwide to fabricate lattice structures. Although AM methods are capable of producing lattice structures with controllable pore shape and size and with high repeatability, they are expensive and time consuming even for fabricating small specimens. Accordingly, developing numerical models, which are able to predict the mechanical properties of lattice structures, can decrease the required experimental measurements as well as the fabrication cost.

The first attempts for modeling the mechanical properties of porous materials go back to the works by Gent and Thomas [1,2], Ko [3], Shaw and Sata [4], Patel and Finnie [5], and Dement'ev and Tarakanov [6]. The main scope of these investigations was to present the elastic modulus of highly porous materials as a function of the relative density. Several attempts were further performed to model the nonlinear as well as linear part of the stress–strain response of porous materials. Two main methodologies were used to model the mechanical behavior of porous materials as well as cellular lattices named unit cell [7–11] and supper cell [12–16] methods.

In the unit cell method, microstructure of a porous material is supposed to be regular by repeating a unit cell in space. Accordingly, only one repeating cell can be used to obtain the mechanical behavior of a porous specimen. Although this modeling approach is computationally efficient, it is suitable for cases where the pore size is smaller than the sample's dimensions. Also, in this method, the effects of the microstructural defects and imperfections cannot be included [17]. To repel these difficulties, the supper cell method is proposed. In this approach, a representative volume element (RVE) of the real porous sample with more geometrical details is used to model the mechanical behavior of a porous specimen. In this regard, to generate geometry of porous materials, several methodologies have been used, among which Voronoi tessellation [15], the method of minimum energy [18], removing or assigning zero stiffness to a number of elements [19], and distributing some pores in a matrix [20] are more popular. Using these models, several attempts were performed to study the microstructural imperfections of porous materials such as irregular cells in shape and size [13–15], non-uniform pore's walls [12,21], curvy and wavy pore's walls [22,23], and microstructural defects [24,25].

* Corresponding author. Tel.: +98 31 3391 2436.
E-mail addresses: m.karamoozravari@me.iut.ac.ir (M.R. Karamooz Ravari), kadkhodaei@cc.iut.ac.ir (M. Kadkhodaei), mohsen.badrossamay@cc.iut.ac.ir (M. Badrossamay), reza.rezaei@me.iut.ac.ir (R. Rezaei).

http://dx.doi.org/10.1016/j.ijmecsci.2014.08.009
0020-7403/

By developing additive manufacturing methods, efforts for fabrication and characterization of cellular lattice structures are increasing. These methods allow to adjust the mechanical properties of lattices by using an appropriate microstructure. Santorinaios et al. [26] fabricated BCC-Z cellular lattice structures using selective laser melting (SLM) from stainless steel. They experimentally investigated the lattices under compression and shear loading. Mines [27] precisely discussed theoretical and experimental issues related to characterization, modeling, calibration, and validation of core cellular materials used in sandwich constructions. McKown et al. [28] fabricated and tested BCC and BCC-Z cellular lattice structures with the use of SLM rapid prototyping technique to characterize the progressive collapse behavior, failure mechanism, and rate-dependent properties of their products. Gorny et al. [29] used some in-situ approaches, including electron backscatter diffraction, scanning electron microscopy, and digital image correlation, to study deformation of a lattice structure produced by SLM. Mines et al. [30] manufactured and characterized BCC micro-lattices made from Ti6Al4V titanium alloy and 316 L stainless steel, as the core material for sandwich panels, using SLM. Gumruk et al. [31] experimentally examined the static behavior of BCC and BCC-Z stainless steel micro-lattice structures manufactured by SLM under several loading types such as compression, shear, tension, and combined loadings. Mines et al. [32] fabricated small sandwich panels with micro-lattice cores with the use of SLM. They analyzed resultant damage under drop weight loading of a steel hemisphere. Brodin and Saarimäki [33] fabricated some lattice truss structures, hollow rectangular tubes, and composites of tubes with an interior of lattice truss structures using SLM. They then tested all samples under tension to compare their mechanical behavior. Campanelli et al. [34] investigated the fabrication of Ti6Al4V micro-lattices with pillar textile unit cells by means of selective laser melting. They also performed compression tests in order to evaluate strength and energy absorption of the lattice truss specimens. Yan et al. [35] produced diamond lattice structures using direct metal laser sintering (DMLS) to evaluate the manufacturability and performance of AlSi10Mg periodic cellular lattice structures.

After successful fabrication of cellular lattice structures, the efforts for modeling their mechanical behavior were increased. Labeas and Sunaric [36] developed a new approach to account for buckling of the lattice struts. Then, they used this method to investigate the structural response and failure process of open lattice metallic cellular cores. Luxner et al. [37] used both 3D and beam finite element models to study the elastic modulus of lattice structures fabricated by rapid prototyping methods. The micro-CT images of the cellular lattice microstructures show some imperfections in the struts of the lattice including diameter variations, micro- or nano-pores, and semi- or non-melted powders. These imperfections affect the mechanical properties of the lattice. Through experimental and computational analyses, Zhou et al. [38] studied deformations in a lattice block structure with a pyramidal core structure and triangulated planar truss faces. They carried out some tension and compression tests on individual struts to capture the effects of the microstructural defects. Using a beam finite element model as well as theoretical approaches, Gumruk and Mines [39] investigated the mechanical behavior of 316 L stainless steel micro-lattice fabricated by selective laser melting under the application of static compression. To consider the microstructural defects in the lattice struts, they attributed the stress–strain response of individual struts to the bulk material. As the elastic modulus obtained from simulation was not satisfactory, they calibrated the stress–strain curve of the individual strut using the elastic part of the lattice. This was used as the correlated curve for modeling the nonlinear region of the response. Smith et al. [40] used finite element simulation to predict compressive response of the body-centered cubic lattice structure and a similar structure with vertical pillars. They used both 3D and beam finite element models in their analysis. To account for defects in the micro-struts, the calibrated stress–strain response of the individual struts provided in [39] was used. Campoli et al. [41] developed some beam finite element models to study the elastic behavior of cellular lattices fabricated by selective laser melting and electron beam melting. Using statistical methods, they implemented irregularities caused by the manufacturing process including structural variations of the architecture. Karamooz and Kadkhodaei [42] developed a beam finite element model for predicting the elastic modulus of Ti6Al4V scaffolds. They also compared the effects of the mechanical properties of the bulk material on the elastic modulus. Ahmadi et al. [43] presented analytical solutions and closed form relationships for predicting the elastic modulus, Poisson ratio, critical buckling load, and yield stress of cellular structures made of the diamond lattice unit cell. They compared the analytical results with those obtained using finite element simulations and experimental measurements for Ti6Al4V specimens fabricated using selective laser melting.

In this paper, the effects of variation in struts' diameter on the elastic modulus as well as collapse stress of cellular lattices is analyzed. To this end, some lattice structures as well as compression test specimens are fabricated using fused deposition modeling to obtain the mechanical compressive behavior of the lattice and bulk material, respectively. To determine variations of the struts' diameter along the length, measurements are done in several points of each strut, and the probability of the diameters is calculated. Then, solid and beam finite element models are developed to obtain the elastic modulus of the lattice. In these models, each strut is divided into a number of intervals to model the random variations of diameter. Using this method, the effects of variation of struts' diameter on the elastic modulus and the collapse stress are assessed with the use of both beam and solid finite element analyses. Solid and beam models are compared in terms of computational time as well as predicted elastic modulus and collapse stress. Moreover, configuration of the deformed structure is determined through experimental observations and finite element models.

2. Experimental procedure

2.1. Fabrication

The cellular lattice structures investigated in this paper are generated by repeating the BCC-Z unit cell are shown in Fig. 1. The nominal diameter of struts is 1.5 mm, and dimensions of

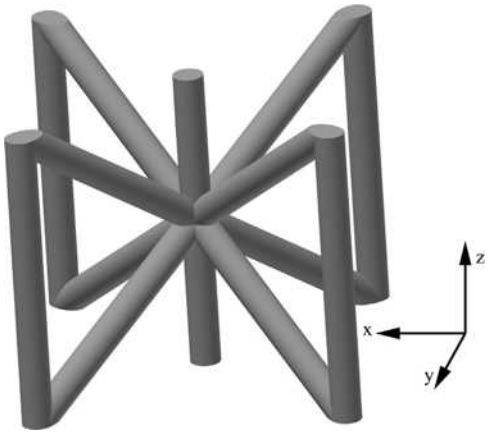

Fig. 1. Three dimensional view of a unit cell.

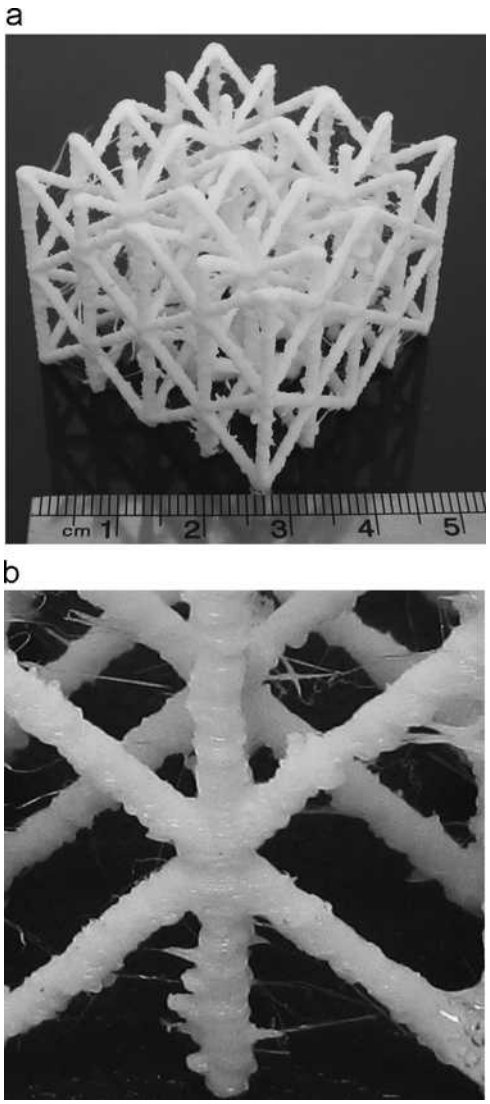

Fig. 2. (a) A PLA cellular lattice structure fabricated by FDM (b) a close view of CLS's struts and joints.

the cellular structure are 36.0 mm × 36.0 mm × 30.21 mm. These dimensions are obtained according to the capabilities of the available AM machine using some designed benchmarks (not presented here). More information about finding capability of the AM machine is provided in [44].

First of all, a three-dimensional (3D) CAD model is extended to provide horizontal two-dimensional (2D) slice information of the sample. The slice data are then sent to the fused deposition modeling (FDM) machine for fabrication. A laboratory extruding-based apparatus, RAPMAN 3.2, is used to fabricate the samples. A polylactic Acid (PLA) filament with the diameter of 3 mm is fed as the raw material. The model is constructed by deposition of material in layers. Once a layer is built, the platform moves down one step in z direction, equal to the specified layer thickness, to deposit the following layer. Fig. 2(a) and (b) respectively shows one of the fabricated cellular lattice structures and a close view of the struts and joints.

As mentioned above, the structure is made layer by layer so the diameter may be different from one layer to another. Consequently, diameter of the struts is measured in several points, and the probability of existing ranges for diameters is determined. This issue will be discussed later in Section 4.

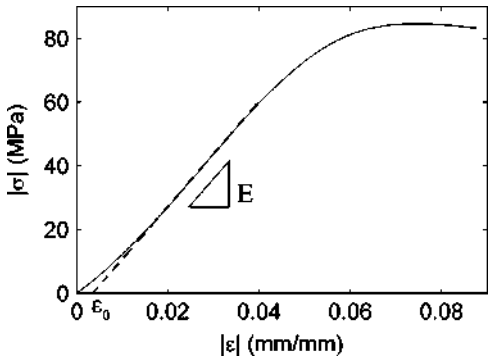

Fig. 3. Experimental and corrected stress–strain curve of the bulk compression specimen.

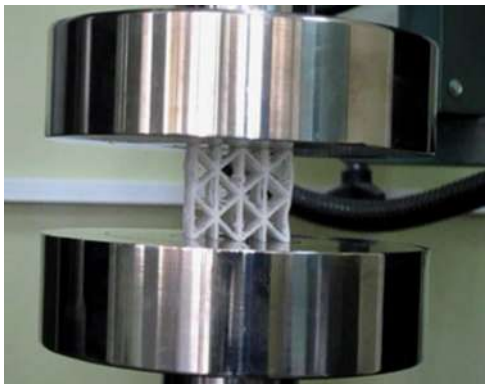

Fig. 4. Compression test of cellular lattice structure.

2.2. Mechanical characterization

Since in AM methods fabrication is carried out by stacking layers in different directions, the produced parts usually exhibit different mechanical properties from cast or wrought materials. For understanding the mechanical property of the fabricated PLA parts, bulk compression specimens are designed according to ASTM D638 [45] and are fabricated by FDM. Simple compression test is then carried out at the strain rate of $2 \times 10^{-4}\,S^{-1}$ using universal SANTAM, STM-50 testing machine. The stress–strain curve of the bulk compression specimen is shown in Fig. 3. As can be seen in this figure, a toe region is obvious in the small strains. To calculate the elastic modulus and to obtain a typical stress–strain curve for simulation purposes, the method presented in ASTM D695 [46] is used. In this method, which is schematically shown in Fig. 3, continuation of the linear region of the curve is intersected by the zero-stress axis. This junction (shown by ε_0 in the figure) is considered as the corrected zero strain point from which all extensions or strains must be measured. Using this method, the elastic modulus of the bulk material in compression is calculated to be 1684.8 ± 144.7 MPa.

To ensure that compression tests are performed under static conditions on the cellular lattice structures, the strain rate of $10^{-5}\,s^{-1}$ is chosen. Fig. 4 shows the manufactured cellular lattice structure in compression test. The obtained stress–strain curve and its correction are shown in Fig. 5, according to which the average elastic modulus (E^*) of 49.07 ± 0.13 MPa and the collapse stress (σ_c^*) of 1.018 MPa are achieved.

3. Finite element modeling

In this paper, both solid and beam finite element models are used to calculate the elastic modulus and the collapse stress of

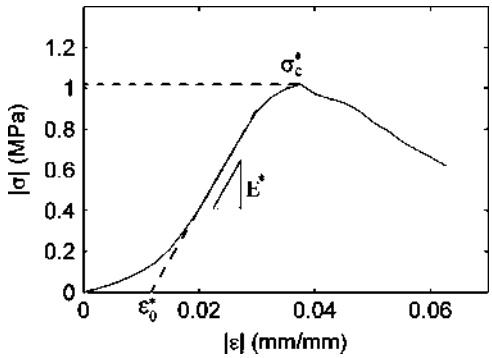

Fig. 5. Experimental and corrected stress–strain curve of the cellular lattice structure.

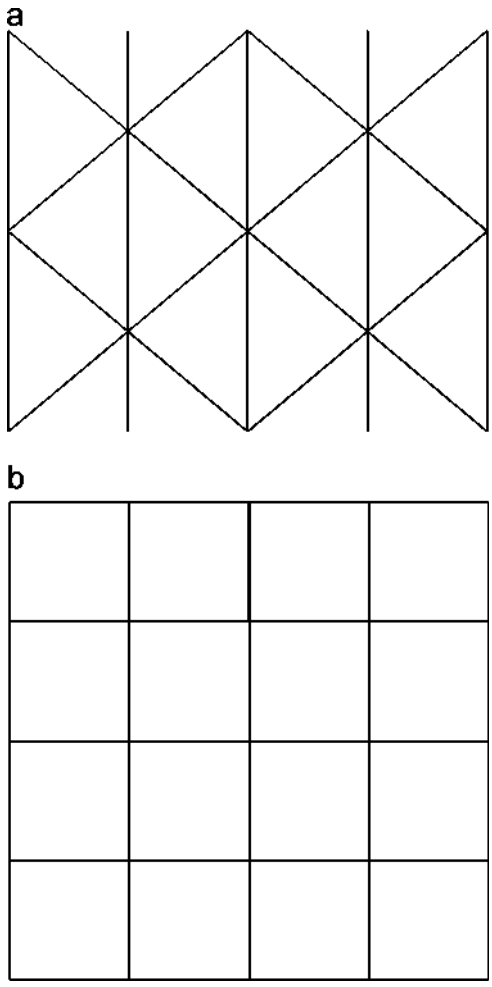

Fig. 6. The wireframe of the cellular lattice (a) front view (b) top view.

cellular lattices. The beam model is computationally efficient while the solid one can model the geometry with more details. In the following sub-sections, details of the models will be discussed. All the simulations are performed by the commercial finite element software ABAQUS/STANDARD.

3.1. Beam finite element model

To generate the beam finite element model, a script is developed through python 6.6.6. The script gets the lattice vertexes as well as their connection as its input to generate the wireframe of the lattice as shown in Fig. 6(a) and (b).

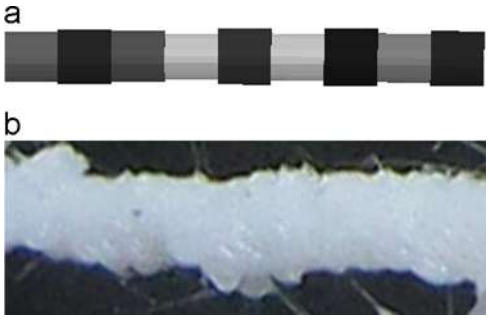

Fig. 7. (a) A strut divided into 9 intervals, and the randomly generated diameters are assigned to the intervals (b) a real strut of the fabricated CLS.

Fig. 8. Generating a solid strut with variable diameter.

Each strut of the lattice is divided into N equally-spaced intervals to be able to model variations in the struts' diameter. Then, the structure is imported into ABAQUS 6.11-1, and a randomly generated diameter is assigned to each interval. The method for generating the random diameters will be presented in Section 3.3. Fig. 7(a) and (b) shows a strut divided into 9 intervals and a real CLS's strut, respectively.

Each interval of the struts is meshed using the three dimensional, shear deformable, quadratic beam element B32. The cross section of the struts is supposed to be circular. The trapezoidal rule is used for integration point i.e. there are 3 and 8 integration points in the radial and circumferential directions, respectively.

3.2. Solid finite element model

A script is developed to generate a solid finite element model of the lattice. To define non-uniformities in the struts' cross section along the length, the space between each two connected vertexes is divided into N intervals. As shown in Fig. 8, in the center of each interval, a point is located at a random distance from the connecting line. Then, a curve is fitted to the generated points, and the curve is revolved to produce the strut. This procedure is repeated for all struts. After modeling the whole structure, two plates are defined at the bottom and top of the structure to remove the overplus parts of the structure which are produced during the modeling process. Fig. 9(a) and (b) shows the overplus part at the conjunction of the struts and the whole solid model, respectively.

The model is meshed using a second- order accuracy tetrahedral continuum element, C3D10M, to be able to capture the complex geometry of the struts especially in the conjunction of the struts and to avoid numerical problems. Fig. 10 shows a close view of the meshed structure at a junction of struts for $N=8$.

3.3. Calculating the struts' diameter at each interval

Since some diameters are more probable, the diameter assignment should be performed according to the probability which is calculated for a range of diameters. To assign a diameter to a strut's interval, an index is attributed to each range of diameters. Then, a set whose members are the indices of the diameter range is generated. Each index is repeated M times, which M is the nearest integer number to the probability of that diameter range so that $\sum M_i = 100$. To generate the diameter of each interval, first, an

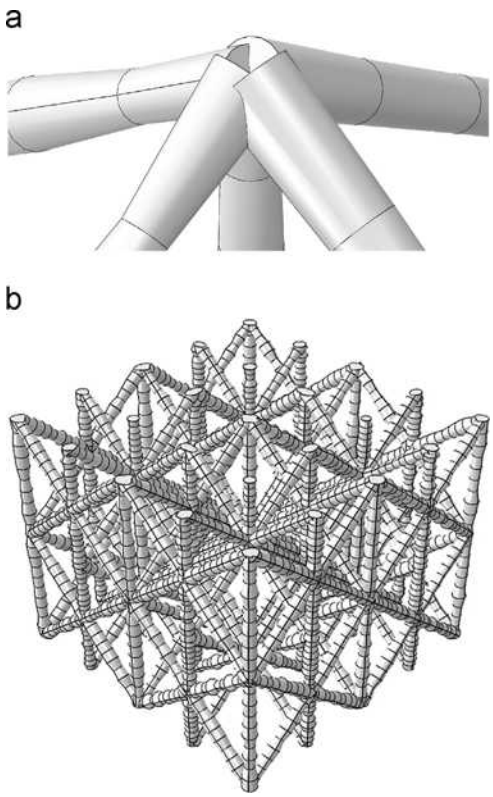

Fig. 9. (a) The overplus of the struts at a conjunction (b) the whole solid model of the structure.

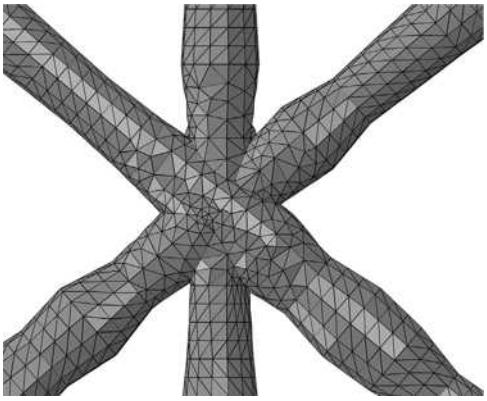

Fig. 10. A close view of the meshed structure at the struts' junction.

integer number between 1 and 100 is randomly generated referred to a member of the indices' set to choose an index. Afterward, a random diameter is calculated in the selected diameter range. It is worth mentioning that, to capture the effects of material concentration at the vertexes, diameter of the struts located at the vertexes is calculated using the four largest diameter ranges.

For a better comparison, a model with a constant cross section along the strut's length is generated too. In this model, the average value of the struts' diameters is assigned to all the struts.

3.4. Boundary conditions

To coincide with the experimental uniaxial compression test, all the translational degrees of freedom on the bottom face of the lattice are fixed while the rotational ones are free. For the upper face of the lattice, all the translational degrees of freedom are fixed except in the loading direction. In the loading direction, all the nodes in the upper face are supposed to move toward the bottom face. The rotational degrees of freedom are all free. Moreover, no boundary condition is applied to the sides of the lattice. Fig. 11 summarizes the above-mentioned boundary conditions schematically.

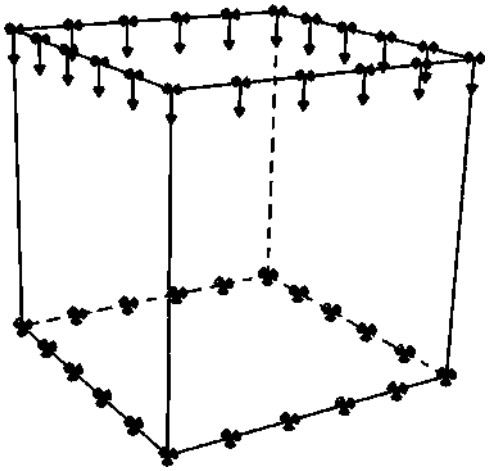

Fig. 11. Schematic of the applied boundary conditions to the cellular lattice.

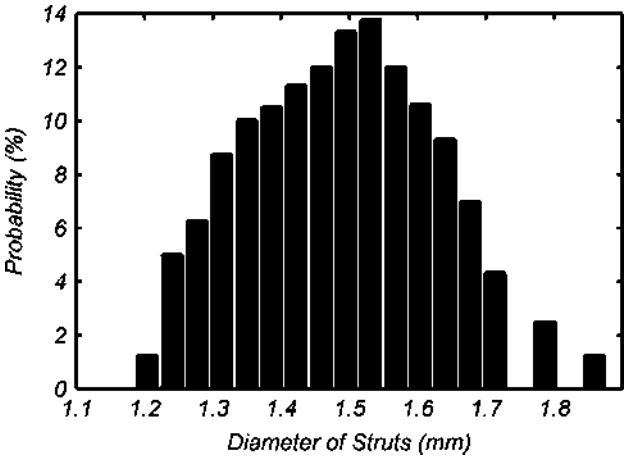

Fig. 12. Probabilities for diameter of struts.

4. Results

As mentioned earlier, the struts' defects and imperfections can affect the mechanical properties of cellular lattices. Due the inherence of AM methods for fabricating cellular lattice structure, the building direction can affect the struts' diameter. Accordingly, the diameter as well as its variation along the strut's length of vertical struts can be different from diagonal ones. This issue depends on the fabrication method. To account for such effects, the diameter variations of vertical and diagonal struts are measured separately and are compared with each other. For the present specimens fabricated by the utilized FDM machine, difference between the diameters of vertical and diagonal struts is negligible. Consequently, in this paper, the same pattern for diameter variations is used for both vertical and diagonal struts. It is worth mentioning that, for cases where this difference is of concern, separate patterns can be used for these two (or more) kinds of built struts. Fig. 12 shows the probability of the ranges of struts' diameter along its length in the form of a histogram. As is seen, the most probable diameter is about 1.5 mm which is the

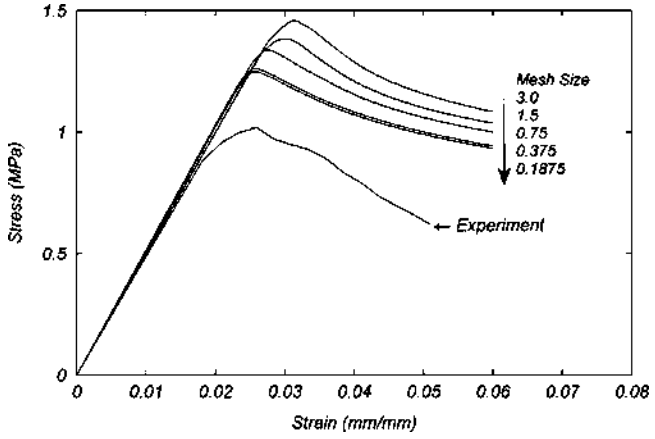

Fig. 13. Stress–strain curve for different values of mesh size and $N=1$.

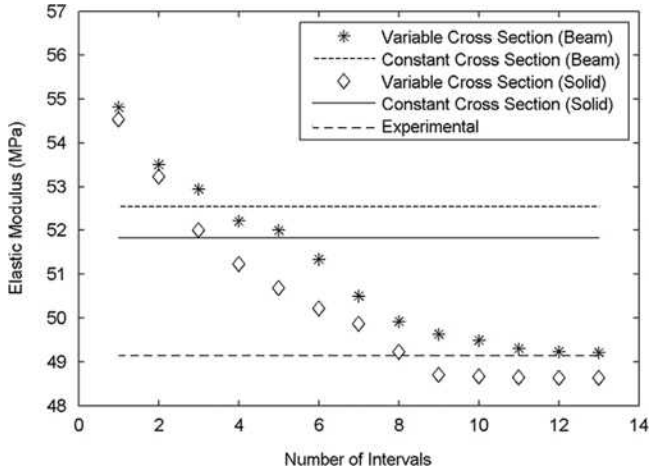

Fig. 14. Variations of the elastic modulus of the lattice with the number of intervals.

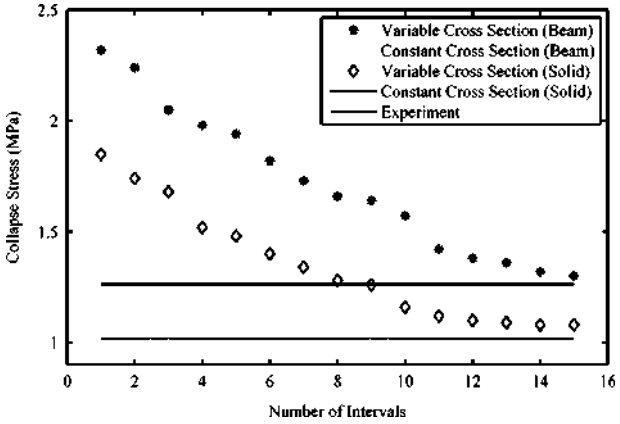

Fig. 15. Variations in the collapse stress of the lattice with the number of intervals.

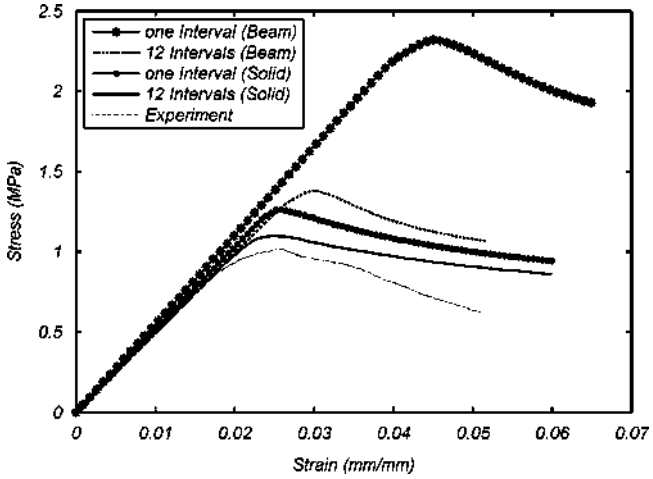

Fig. 16. Stress–strain curve for the beam and solid finite element models with one and 12 intervals.

designed value. This histogram is used to construct the finite element models for considering the struts' diameter variation.

All the following simulations are performed on a 2 Intel Xeon X5670 (12 core), 2.93 GHz processors with 24 cores and 24 GB RAM.

Before reporting the results, a mesh-sensitivity study is performed for each value of N. The results (not presented here) show that the difference between the average stress–strain curve for 5 and 6 beam elements per interval is negligible. Therefore, in all beam models, 5 elements are used to mesh each beam. For solid model, a fine mesh is needed to capture details of the geometry especially in the vicinity of the vertexes. Also, to model the variation of the struts' cross section, a fine mesh should be used. Nevertheless, using a fine mesh can increase the required memory as well as computational time. Shown in Fig. 13 is the stress–strain curve of the PLA cellular lattice for different values of mesh size when $N=1$. As shown in this figure, although the elastic region varies slightly with the mesh size, the effect of mesh size on the nonlinear region is more severe. The difference between nonlinear regions is negligible for 0.375 and 0.1875 mesh sizes, so the mesh size value of 0.375 is used for this simulation. A similar trend is followed for each value of N to be assured that the mesh size does not significantly affect the results.

As the struts' diameter is assigned randomly, the results may be different from one model to another. To reduce the randomness effects, 20 models are generated and solved for each value of N, and the average stress–strain curve is reported. Fig. 14 shows the elastic moduli of the lattice versus the number of intervals for both solid and beam models with constant and variable cross sections. As shown in the figure, by increasing the number of intervals, the elastic modulus of the lattice gets closer to the experimentally measured value. The maximum error occurs for one interval and in the beam model. The error is decreased to values smaller than 1.5% for at least 9 intervals in both beam and solid variable cross section models.

Fig. 15 shows variations of the collapse stress with the number of intervals for both beam and solid finite element models. The trend of changes is similar to the one presented for the elastic modulus. In this case, both models over-predict the collapse stress, and the predictions of beam model are higher than those obtained using solid model. Maximum error compared with the experimental results is 127.9% for one interval beam model. The error decreases by increasing the number of intervals. The minimum error is about 6.1% for solid model. This value is about 27.7% for the beam model.

5. Discussion

5.1. Stress–strain behavior

The stress–strain responses for beam and solid finite element models with 1 and 12 intervals are presented in Fig. 16. Referring to this figure, the beam model prediction is not satisfactory for one interval. The collapse stress and strain are higher than the

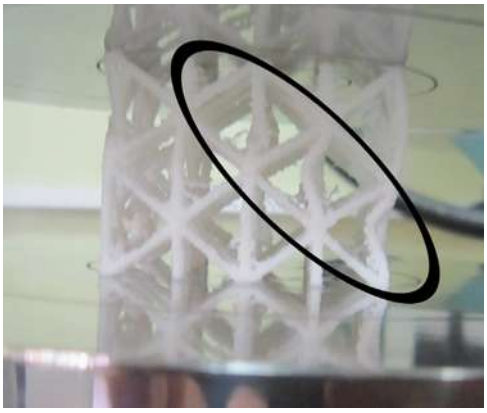

Fig. 17. Deformed configuration of the lattice under the strain of 3.2%.

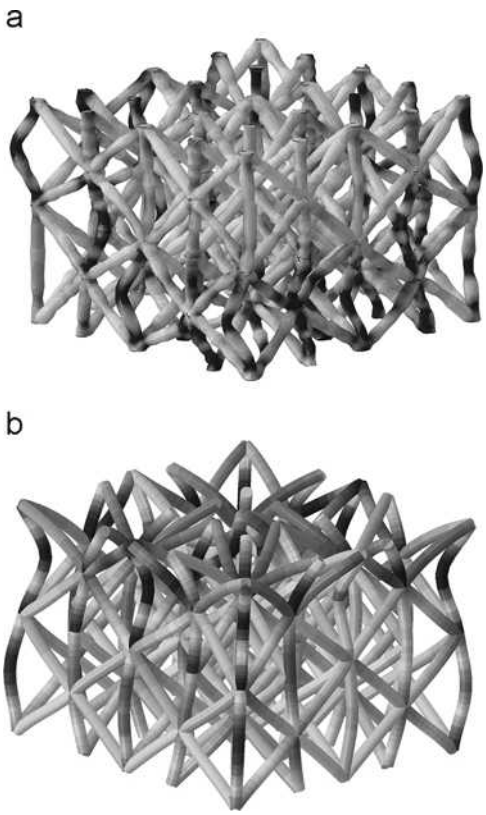

Fig. 18. Predicted deformed configuration of the lattice at the strain of 3.2% using (a) solid and (b) beam finite element model.

experimental findings. By increasing the number of intervals, the collapse stress and its relating strain get closer to the experimentally measured values. The prediction of solid model with just one interval is better than that of the beam model with 12 intervals. The predictions by the solid model with 12 intervals are much better fitted with the experimental ones. Referring to Figs. 14 and 15, by increasing the value of N more than 12, slight improvements in both elastic moduli and collapse stress are achieved.

For a better comparison, the obtained results using constant cross section models are also considered and depicted in Figs. 14 and 15. The constant cross section beam model predicts the elastic modulus and collapse stress with a difference of about 7% and 61.1%, respectively. These values are about 6% and 23.9% for the constant cross section solid model. In all the models, the elastic modulus as well as collapse stress predicted by the beam model is higher than that by the solid model. It might be due to stress concentration in some regions such as vertexes in the solid model in comparison with the beam model.

In terms of the computational time, the solid models are more inefficient than the beam models. As the number of intervals increases, a finer mesh is needed to capture the geometrical details. If the elastic modulus is of importance, one can use beam finite element models for predicting the elastic modulus of cellular lattice structures with the struts' aspect ratios (strut's diameter divided by strut's length) of up to 1/8 because the Timoshenko beam theory is valid for this range of aspect ratio with a constant cross section. But, for a good prediction of plastic region, a solid finite element model should be used. In this regard, based on the desired accuracy, either solid model with a small number of intervals or beam model with larger values of N can be used.

5.2. Deformation of the lattice

The deformed configuration of the fabricated cellular lattice at the strain of 3.2% is presented in Fig. 17. By applying compression on the lattice, elastic deformation is started. The stress contours (not presented here) show that, in the elastic regime, almost all the compressive load is carried by the vertical struts. By increasing the applied force, the vertical struts start to buckle and a shear band initiates. More compression causes the formation of plastic hinge in the diagonal struts and near the vertexes. This phenomenon starts in the diagonal struts, which connect the boundaries of the shear band region. As another observation, buckling of the vertical struts starts in the struts placed in the corners of the lattice. Referring to Fig. 17, the shear band forms parallel to the diagonal struts.

Fig. 18(a) and (b) shows the deformed configuration of the lattice at the same strain presented in Fig. 16 using solid and beam finite element models, respectively. The predictions by solid model are reasonably well fitted by experimental ones while the beam model predictions are not satisfactory. Notice that since the deformed configuration of several intervals beam model is similar to the beam model with one interval, so the latter is just presented in Fig. 18(b) for a better view.

6. Conclusion

In this paper, some cellular lattices are fabricated by FDM and are tested in compression to obtain the elastic modulus and the collapse stress of the lattice. The struts' diameter is measured in several points of each strut, and the probability of the diameters is calculated. To obtain the material parameters of the bulk material, some compression test samples are fabricated and tested too. Then, finite element models based on beam and solid elements are developed to predict the elastic modulus as well as collapse stress of the lattice. To do so, different models with variable and constant cross sections are generated using both beam and solid models. The results show that, to obtain a good accuracy, it is necessary to model the cross section variations along the strut's length. It is also shown that the solid model predicts a lower mechanical stress–strain curve than that by the beam model. It might be as a result of stress concentration at some regions in the solid model in comparison with the beam model. Finally, the stress–strain curves and deformed configurations obtained using beam and solid finite element models are compared with experimental findings. According to the obtained results, at least ten and twelve intervals should be considered for each strut to achieve reasonable elastic modulus and collapse stress, respectively. The results demonstrate that the solid models are more accurate even with just one interval. However, the beam models are more computationally

efficient. The decision on which method is suitable should be made based on the desired accuracy and computational cost.

Acknowledgment

All the simulations are performed in National High-Performance Computing Center of Isfahan University of Technology. The authors would also like to thank Dr. Ashrafizadeh for making it possible to use the facilities of National High-Performance Computing Center.

References

[1] Gent AN, Thomas AG. The deformation of foamed elastic materials. J Appl Polym Sci 1959;1:107–13.
[2] Gent AN, Thomas AG. Mechanics of foamed elastic materials. Rubber Chem Technol 1963;36:597–610.
[3] Ko WL. Deformations of foamed elastomers. J Cell Plast 1965;1:45–50.
[4] Shaw MC, Sata T. The plastic behavior of cellular materials. Int J Mech Sci 1966;8:763–71.
[5] Patel MR, Finnie I. Structural features and mechanical properties of rigid cellular plastics. J Mater 1970;5:909–32.
[6] Dement'ev AG, Tarakanov OG. Model analysis of plastics foams of the polyurethane type. Polym Mech 1970;6:744–9.
[7] Gibson LJ, Ashby MF. The mechanics of three-dimensional cellular materials. Proc R Soc A 1982;382:43–59.
[8] Hodge AM, Dunand DC. Measurement and modeling of creep in open-cell nial foams. Metall Mater Trans A 2003;34A:2553–63.
[9] Chen T-J, Huang J-S. Creep-buckling of open-cell foams. Acta Mater 2009;57:1497–503.
[10] Hutchinson RG, Fleck NA. Microarchitectured cellular solids—the hunt for statically determinate periodic trusses. ZAMM 2005;85:607–17.
[11] Sullivan RM, Ghosn LJ, Lerch BA. A general tetrakaidecahedron model for open-celled foams. Int J Solids Struct 2008;45:1754–65.
[12] Grenestedt JL, Bassinet F. Influence of cell wall thickness variations on elastic stiffness of closed-cell cellular solids. Int J Mech Sci 2000;42:1327–38.
[13] ROBERTS AP, GARBOCZI EJ. Elastic moduli of model random three-dimensional closed-cell cellular solids. Acta Mater 2001;49:189–97.
[14] Roberts AP, Garboczi EJ. Elastic properties of model random three-dimensional open-cell solids. J Mech Phys Solids 2002;50:33–55.
[15] Van der Burg MWD, Shulmeister V, Van der Geissen E, Marissen R. On the linear elastic properties of regular and random open-cell foam models. J Cell Plast 1997;33:31–54.
[16] Zhu Y, Dui G. A model considering hydrostatic stress of porous niti shape memory alloy. Acta Mech Solida Sin 2011;24:289–97.
[17] Gan YX, Chen C, Shen YP. Three-dimensional modeling of the mechanical property of linearly elastic open cell foams. Int J Solids Struct 2005;42:6628–42.
[18] Weaire D, Phelan R. A counter-example to Kelvin's conjecture on minimal surfaces. Philos Mag Lett 1994;69:107–10.
[19] Panico M, Brinson LC. Computational modeling of porous shape memory alloys. Int J Solids Struct 2008;45:5613–26.
[20] Alvarez P, Mendizabal A, Petite MM, Rodríguez-Pérez MA, Echeverria A. Finite element modelling of compressive mechanical behaviour of high and low density polymeric foams. Mater Werkst 2009;40:126–32.
[21] Zhu HX, Chen CY. Combined effects of relative density and material distribution on the mechanical properties of metallic honeycombs. Mech Mater 2011;43:276–86.
[22] Grenestedt JL. Influence of wavy imperfections in cell walls on elastic stiffness of cellular solids. J Mech Phys Solids 1998;46:29–50.
[23] SIMONE AE, GIBSON LJ. The effects of cell face curvature and corrugations on the stiffness and strength of metallic foams. Acta Mater 1998;46:3929–35.
[24] Chen C, Lu TJ, Fleck NA. Effect of imperfections on the yielding of two-dimensional foams. J Mech Phys Solids 1999;47:2235–72.
[25] Luxner MH, Stampfl J, Pettermann HE. Nonlinear simulations on the interaction of disorder and defects in open cell structures. Comput Mater Sci 2009;47:418–28.
[26] Santorinaios M, Brooks W, Sutcliffe C, Mines R. Crush behaviour of open cellular lattice structures manufactured using selective laser melting. WIT Trans Built Environ 2006;85:481–90.
[27] Mines R. On the characterisation of foam and micro-lattice materials used in sandwich construction[1]. Strain 2008;44:71–83.
[28] McKown S, Shen Y, Brookes W, Sutcliffe C, Cantwell W, Langdon G, et al. The quasi-static and blast loading response of lattice structures. Int J Impact Eng 2008;35:795–810.
[29] Gorny B, Niendorf T, Lackmann J, Thoene M, Troester T, Maier H. In situ characterization of the deformation and failure behavior of non-stochastic porous structures processed by selective laser melting. Mater Sci Eng: A 2011;528:7962–7.
[30] Mines R, Tsopanos S, Shen Y, Hasan R, McKown S. Drop weight impact behaviour of sandwich panels with metallic micro lattice cores. Int J Impact Eng 2013;60:120–32.
[31] Gümrük R, Mines R, Karadeniz S. Static mechanical behaviours of stainless steel micro-lattice structures under different loading conditions. Mater Sci Eng: A 2013;586:392–406.
[32] Mines R., Tsopanos S., Shen E., McKown S., Cantwell W., Brooks W., et al.. On the performance of micro-lattice structures as core materials in sandwich panels subject to low velocity impact. In: Proceedings of the 17th international conference on Composite materials (ICCM-17). Edinburgh, UK; 2009. p. 27–31.
[33] Brodin H., Saarimäki J. Mechanical properties of lattice truss structures made of a selective laser melted superalloy. In: 13th international conference on fracture. Beijing, China; 2013.
[34] Campanelli S, Contuzzi N, Ludovico A, Caiazzo F, Cardaropoli F, Sergi V. Manufacturing and characterization of Ti6al4v lattice components manufactured by selective laser melting. Materials 2014;7:4803–22.
[35] Yan C, Hao L, Hussein A, Bubb SL, Young P, Raymont D. Evaluation of light-weight Alsi10mg periodic cellular lattice structures fabricated via direct metal laser sintering. J Mater Process Technol 2014;214:856–64.
[36] Labeas GN, Sunaric MM. Investigation on the static response and failure process of metallic open lattice cellular structures. Strain 2010;46:195–204.
[37] Luxner MH, Stampfl J, Pettermann HE. Finite element modeling concepts and linear analyses of 3d regular open cell structures. J Mater Sci 2005;40:5859–5866.
[38] Zhou J, Shrotriya P, Soboyejo WO. On the deformation of aluminum lattice block structures: from struts to structures. Mech Mater 2004;36:723–37.
[39] Gumruk R, Mines RAW. Compressive behaviour of stainless steel micro-lattice structures. Int J Mech Sci 2013;68:125–39.
[40] Smith M, Guan Z, Cantwell WJ. Finite element modelling of the compressive response of lattice structures manufactured using the selective laser melting technique. Int J Mech Sci 2013;68:28–41.
[41] Campoli G, Borleffs MS, Amin Yavari S, Wauthle R, Weinans H, Zadpoor AA. Mechanical properties of open-cell metallic biomaterials manufactured using additive manufacturing. Mater Des 2013;49:957–65.
[42] Karamooz RavariM., Kadkhodaei M.. Finite element modeling of the elastic modulus of Ti6al4v scaffold fabricated by SLM. In: Proceedings of the fifth biot conference on poromechanics, ASCE. p. 1021–1028.
[43] Ahmadi SM, Campoli G, Amin Yavari S, Sajadi B, Wauthle R, Schrooten J, et al. Mechanical behavior of regular open-cell porous biomaterials made of diamond lattice unit cells. J Mech Behav Biomed Mater 2014;34:106–15.
[44] Rezaie R, Badrossamay M, Ghaie A, Moosavi H. Topology optimization for fused deposition modeling process. Procedia CIRP 2013;6:522–7.
[45] ASTM, standard test method for tensile properties of plastics, in: D 638-03, United States, 2003.
[46] ASTM, standard test method for compressive properties of rigid plastics, in: D 695-02a, United States, 2002.